Identification of blowing snow particles in images from a multi-angle snowflake camera

The Cryosphere #tc-2018-248

M. Schaer, C. Praz and A. Berne

May 13, 2019

Responses to reviewers

We would first like to apologize for the delay in preparing the revised version. We then thank the reviewers for their constructive comments which greatly helped improve the manuscript. In the present document, we provide our responses to the comments of the two reviewers. The comments of the reviewers are reported in *italic*, our responses in normal font and the corresponding modifications in the manuscript in blue. Page and line numbers referred to in our responses correspond to the version with changes highlighted.

Reviewer 1

General comments

1. *Section 4.1 describes the selection of features used in the classification. The author use four categories of descriptors and mention in Sect. 4.1 which descriptor was finally kept within each category. However, the selection of the descriptors is only qualitatively described and only the final selection is given. The authors should better justify the choice of the descriptors based on quantitative results. Figures 5 and 6 could certainly help but they are never described in the text.*

   Section 4.1 describes how the features are selected using an objective quantitative criterion, but we added text to better explain the approach and the information presented in Fig.5 (p.10, l.15-24):
   The marginal distributions of the selected descriptors for the training set are shown in Figure 6 to provide an idea of their respective magnitude and variability, as well as to illustrate their discrimination potential. As noted above, the image frequency is the most informative descriptor to distinguish blowing snow and precipitation.
   In summary, four descriptor categories (related to particle size, particle geometry and particle distribution within the image as well as image frequency) have been defined to distinguish images collected during blowing snow or snowfall, based on 20 the expected differences in particle size and concentration between the two. A number of descriptors were estimated

from each image by computing various quantiles and moments of the distributions of geometric properties of the particles in the considered image. One descriptor from each of the four categories defined above (listed in Table 2) was then selected to be further used for classification as the one maximizing the inter-clusters over intra-clusters" distance defined in Eq. 1.

2. *It would be also interesting to associate the choice of the final descriptors with physical processes occurring during wind-driven snow transport. For example, the choice of the descriptors related to the size and shape of the particles can be associated with the fragmentation of particles (Comola et al. 2017). Comola, F., Kok, J. F., Gaume, J., Paterna, E., Lehning, M. (2017). Fragmentation of wind blown snow crystals. Geophysical Research Letters, 44(9), 4195-4203.*

   We thanks the reviewer fro this suggestion, that we have added in the text in the beginning of Section 3.2 (p.7, l.27-29):
   Because of the fragmentation of ice crystals when hitting the ground surface (e.g. Comola et al., 2017), blowing snow is expected to be characterized by much smaller particle size and much higher particle concentration than snowfall (e.g. Nishimura and Nemoto, 2005; Naaim-Bouvet et al., 2014).

3. *The authors are presenting the results of their method in Section 5. This section contains 1 table and 5 figures for a total of 9 lines of text. I understand that this paper is centered around the description and evaluation of the identification method but the authors should provide a more exhaustive description and discussion of the results that they decided to show to illustrate the use of their method. For example, Figure 11 is quite interesting and should be analyzed more in details by the authors. They could add on this figure the meteorological conditions (wind speed, precipitation) to better explain the transition from a precipitation event to a blowing event.*

   We have revised and significantly extended Section 5 to provide more description and analysis of the results presented in the various figures (see p.16-21).

4. *The same apply to Figure 12. Can the authors comment on the different particle size distribution? For blowing snow particles, how does it compare with particle size distribution measured with Snow Particle Counters (Sato et al., 1993)?*

   We have added a few paragraphs at the end of the new Section 5 to discuss the comparison between the size distribution obtained from MASC images and size distributions based on SPC reported in the literature (see p.20-21).

Specific comments

1. *P 2 L 9: present weather have also been used to monitor drifting and blowing snow near the surface (Bellot et al. , 2011).*
   Bellot, H., Trouvilliez, A., Naaim-Bouvet, F., Genthon, C., Galle, H. (2011). Present

weather-sensor tests for measuring drifting snow. Annals of Glaciology, 52(58), 176-184.

We thank the reviewer for this relevant reference, that was added (p.2, l.10).

2. *P 2 L 18-20: Naaim Bouvet et al. (2014) developed a automatic method to estimate the occurrence of snowfall as well as snowfall amount during blowing snow events using measurements from photoelectric sensors. It could be interesting to mention this study in the introduction since it dealt with topics similar to the ones presented in this paper.*
Naaim-Bouvet, F., Bellot, H., Nishimura, K., Genthon, C., Palerme, C., Guyomarch,G., Vionnet, V. (2014). Detection of snowfall occurrence during blowing snow events using photoelectric sensors. Cold Regions Science and Technology, 106, 11-21.

   We thank the reviewer for this relevant reference, that was added (p.2, l.20 + p.7, l.29).

3. *P 4 L 4: the expression "exceptionally important" is rather unclear and the authors should provide typical values of the image frequency during blowing snow events.*

   We modified the sentence to be more clear (p.5, l.5):
   It was noticed that during strong blowing snow events, the number of images captured by the MASC was much larger than during precipitation events (more than 1 image per second, see Fig. 6).

4. *P 4 L 15-16: we can expect different properties (size, shape and complexity) for the fresh-wind blown snow particles coming from the edges of the DFIR compared to more classic blown snow particles that have been exposed to transport in saltation and turbulent suspension. Can the author comment about it?*

   The new Figure 14 is similar to Figure 7 and presents the distributions of the four selected descriptors, for the entire Antarctic and Alpine data sets, distinguishing pure precipitation and pure blowing snow. These distributions illustrate the differences between blowing snow particles in the two data sets: they appear less fragmented (larger size and fractal index), less scattered within the images (larger distance transform) and with lower image frequencies in Davos than in Dumont d'Urville. This has been added in the text (p.18, l.13 - p.20, l.5):
   Considering the full Antarctic and Alpine data sets, it is interesting to analyze the potential differences in their characteristics. Figure 14 presents the distributions of the four descriptors as in Figure 6, but estimated from the entire data sets and not only the training sets. It can be seen that while the differences are limited for precipitation (slightly more frequent and larger in Davos than in Dumont d'Urville), they are significant for blowing snow: the blowing snow particles appear less fragmented (larger size and fractal index), less scattered within the images (larger distance transform) and with lower image frequencies in Davos. It should be recalled that the MASC was located in a wind-protecting fence in Davos, so first the occurrence of blowing snow is much smaller (0.6 vs 36.5%), and second it is likely related to fresh snow blown away from the top of the nearby fence.

5. *In addition, the authors should comment on the potential deposition of blowing snow particles from the surrounding crests. Is it something that can be observed at the experimental site above Davos?*

   We discussed with colleagues involved in field measurements at the Davos location, and it is not clear if blowing snow particles from the surroundings could deposit or not into the MASC. So unfortunately, we cannot provide a reliable answer to this question.

6. *P 6 L3-7: The beginning of Section 3.1 contains a brief description of the MASC. Other technical details are provided at different places in Sections 1, 2 and 3. I recommend the author to create in Section 2 a sub-section dedicated to the presentation of the MASC and summarizing the main characteristics of the instrument. In this subsection, it would be interesting to add more details regarding the MASC image frequency since it is used by the authors in their image classification method. What is the maximal frequency of the instrument? How does in depend on the particle concentration? To my knowledge, it is the first time the MASC is used to characterize blowing snow particles.*

   A new sub-section (2.1) describing the MASC has been added (p.3-4).

7. *It would be interesting if the authors can briefly compare the characteristics of the MASC and the Japanese Snow Particle Counters (SPC) (Sato et al., 1993) in terms of particle characterizations. The SPC can be currently considered as the reference device for blowing snow measurements (fluxes and particle size distribution).*
   Sato, T., Kimura, T., Ishimaru, T., Maruyama, T. (1993). Field test of a new snow-particle counter (SPC) system. Annals of Glaciology, 18, 149-154.

   See response above.

8. *P 6 L 31-33: The authors computed quantiles and moments of the distribution of the considered feature. What are the typical numbers of particles on an image in the different situations: blowing snow, precipitation, and mixed situation?*

   The number of particles on an image is not a descriptor that has been selected for the classification, so it was not analyzed. We can however mention that:

   - For precipitation: from 1 particle (ideal case) to several (maybe 10) in case of high intensity snow.
   - For blowing snow: from several to one hundred.
   - For mixed case: no typical values.

9. *P 9 L 11: the authors use the term "soft clustering" and the term "hard clustering" at P 10 L 24. These 2 terms can be indirectly understood when reading the text but I recommend the other to include in the text one or two sentences that clearly define these 2 terms.*

We have specified the meaning of these two terms (p.11, l.14 and p.12, l.22).

10. *P 10 L 9: it is not clear why the authors decided to remove exactly 80 data points (images?) from the training dataset.*

    We removed 80 points to have exactly balanced classes in the training set, as explained on p.12, l.5-9.

11. *P 13 L 9-10: How do the authors justify the choice of having 10%*

    The choice of the quantiles 10 and 90% is indeed somehow arbitrary. This means that we assume about 10% of images not corresponding to pure precipitation or blowing snow, which appears reasonable from the bottom plot of Figure 9. It should also be noted that this threshold can be adapted to the user's need/objective. This is now mentioned in the text (p.15, l.17-19):
    This value is qualitatively supported by the distribution shown in Figure 9. It can be changed by the user to be more (increasing it) or less (decreasing it) strict on the classification as pure blowing snow or pure precipitation, depending on the intended application.

12. *P 13 L 15-17: The authors computed an index of mixing for each image as well as an index average among the 3 images with a given time identifier. Can the authors comment on the variability of the value of the index among the 3 images for a given time? Is their classification methods providing consistent results among the 3 cameras for a given time? What are the reasons for the potential differences between the images?*

    As mentioned on p.15, l.26-27, the values of the normalized angle from the three views can be averaged to characterize a given triplet with a single normalized angle value (used in Figure 13 for instance). In addition, we computed the range (defined as max - min) for each triplet and it appeared limited (median of about 0.08 in Davos and 0.05 in Dumont d'Urville). This was added in the text (p.15, l.27-29):
    The median of the range (max - min) covered by the ψ values from the three individual views is about 0.08 in Davos and 0.05 at Dumont d'Urville, indicating a limited variability between the three views.

13. *P 13 Table 3: as mentioned later in the text (P 15 L 12-13), it would be really relevant for the reader to provide as well the percentages expressed in terms of time. The percentage in terms of images are difficult to interpret since they depends on the image frequency that changes with time.*

    As the MASC is not regularly sampling in time (falling particles trigger the instrument), there is no direct link between the percentage of images and the percentage of time.

Technical comments

1. *P 2 L11: the references should be written (Palm et al, 2011) and (Gossart et al., 2017)*

   Done.

2. *P 10 L 4: the signification of the variables used in Eq 2 should be given in the text.*

   Thanks for spotting the issue, we have added the definition of the variables and also moved equation 2 earlier the text (p.11, l.5-7).

3. *Figure 2: it would be interesting to show the period selected as blowing snow and precipitation on the upper graph of Fig. 2 Maybe add lines showing the median values of wind speed and MASC image frequency that were used to identify the different events.*

   Figure 2 is now Figure 3. In the top plot of Figure 3, we indicated the days (as individual time steps would not have been visible) during which the blowing snow and precipitation images were selected. We also used different markers for blowing snow and precipitation point sin the bottom plots.

4. *Figure 2: please indicate at which height above the surface the wind speed is taken.*

   The anemometer at Dumont d'Urville was at 10 m above the ground. This is now mentioned in the caption of Figure 3.

5. *Figure 3: it is very difficult to identify the blowing snow particles due their size. Could the author insert a zoom over a specific region of the image containing blowing snow particles? It would be also useful to include a scale on the images to allow the reader to better estimate the size of particles.*

   Figure 3 is now Figure 4. We have changed the last panel to improve the visibility of the particles in the MASC images. The dimension of the image in pixel and size was been added in the caption.

6. *Figure 4: a scale would be also useful on the images.*

   See previous item.

7. *Figure 7: the labels and legends on the graphs are hard to read and should be made larger.*

Figure 7 is now Figure 8. We are sorry for this, the labels and legend font size has been increased.

8. *Figure 12: mention from which field campaign are taken these data.*

   Figure 12 is now Figure 15. The data were taken from both locations, as now indicated in the caption.

9. *Figure B1: It would be interesting to better highlight on the binary image the artifacts*

   As this figure is in an appendix, we decided to focus on the consistency in the color scheme to better illustrate the different steps of the processing on MASC images.

Reviewer 2

1. *Perhaps it is not crucial, but I am a bit anxious that advanced knowledge of statistics are required to follow the whole contents of this manuscript. In fact, classification procedures are explained considerably careful and I have also learned a bit with the textbook. However, it was still far from satisfactory to follow all of them. They are highly professional and large number of technical terms appears. I appreciate very much if the authors kindly consider the readers who are not so familiar with statistics.*

   We have added text in Section 3.2 and Section 4 to better describe and explain the approach for readers who are not experts in classification and machine learning.

2. *Probably it is a good idea to add following two references, such as in the introduction part. Naaim-Bouvet, F. et al., Detection of snowfall occurrence during blowing snow events using photoelectric sensors, CRST, 106, 11-22, 2014. Nishimura, K., and Nemoto, M., Blowing snow at Mizuho station, Antarctica, Philosophical Transactions of the Royal Soc. of London, A, 363 1647-1662, 2005. The former tried to measure the snowfall amount under the blowing snow condition and the latter showed the snow particle size distribution with SPC and mentions the possibility to detect snowfall.*

   We thank the reviewer for these relevant references, that were added (p.2, l.19-20).

3. *Page 2, Line 6: "The present study focuses on ... more than 2m above ground." This means when the measurements height is getting lower or much higher, new criteria for classification should be set at each time?*

   As indicated in the conclusion (p.23, l.12-15), there is no guaranty that the fitted GMM (and subsequent classification) is fully relevant for MASC images collected in a potentially very different population of blowing snow particles. We therefore recommend to retrain the algorithm if this is the case.

4. *Page 2, Line 22: I wonder the resolution of 33.5 μm is enough to detect the small particles? It is well known that as the position is getting higher, smaller particles will be dominant in the blowing snow. Although the minimum bin in Figure 12 looks 100 μm, measurement in Antarctica indicates diameter less than 100 μm shows the maximum even at the height of 10 cm (Nishimura, K., and Nemoto, M.: 2005).*

   We agree with the reviewer that the MASC resolution (and the image processing) result in the fact that the small blowing snow particles cannot be seen by the MASC. We however think that it is still relevant to be able to distinguish blowing snow and precipitation images at a high temporal resolution. Text has been added at the end of Section 5 to compare size distributions derived from MASC and from SPC (p.19-22).

5. *Page 2, Line 34: I am a bit anxious whether manually-built validation set is satisfactory accurate. Possible error included should be also discussed.*

   AS in many applications, the reference data set cannot be totally free of any error. But we did our best to be strict in the manual identification, and this type of manual classification is a standard approach in machine learning. We added a specific mention of this possible remaining uncertainty in the text (p.5, l.21).

6. *Page 3, Line 13: Same questions listed above. Subsets of pure precipitation and pure blowing snow images were manually selected. I appreciate the authors' efforts very much, but is it perfect?*

   See previous.

7. *Figure 1: Not only the pictures but also a schematic picture of MASC which shows the basic will be helpful.*

   A subsection presenting the MASC was added (Section 2.1, p.3-4).

8. *Page 4, Line 5: Explanations about the MASC should be done before "2. Data sets". Particularly, it should be mentioned here that images are captured when the motion of particles are detected in the field of vision. Otherwise, readers are not able to recognize the meaning of "MASC image frequency" and the importance as one of the descriptors.*

   See previous item.

9. *Figure 3: I dont understand what do you mean by this figure, probably because I did not follow the procedure precisely. Yellow points shown in "Raw image" and "Median filter" do not corresponds to the blowing snow particles? Then, no particles are shown in the "Binary image"; that is blowing snow particles disappear in the final image. Is this correct? On the other hand, precipitation particles remain in the final image as shown in Figure 4?*

   We are sorry that the figures were not well readable. We have updated these figures (now Figure 4 and 5) to improve the contrast and make the identified (blowing sow or precipitation) particles more visible.

10. *Figure 4: This figure looks similar to Figure B1. Are there any different meanings? Figure caption of B1 is much clearer than the one of Figure 4. Same explanation should be done in Figure 4 as well.*

    Figure B1 illustrates a case for which the median filter is not able to remove all background features because of fast changing background conditions, justifying the use of an additional filtering to obtain the final binary image.

11. *Page 10, Equation (2): Notations of D, T and μ(?) should be defined. I suppose μ(?) is not the same as the one in equation (1). Please note that some of the symbol are not readable in the review.*

    Thanks for spotting the issue, we have added the definition of the variables and also moved equation 2 earlier the text (p.11, l.5-7).

12. *Figures 5, 6, 7, 8, 9 and 12; Please make the label of both axes much lager and clearly. It is hard to recognize what is specified respectively.*

    We have increased the font size for labels and legends in the different figures.

13. *Page 13, line 20: Perhaps "850'000" should be expressed as "8.5x10^4".*

    Done.

14. *Page 13, line 24: Similar particle size distributions are found Nishimura and Nemoto (2005) as well. However, the measurements with SPC revealed that the population of smaller particles than 100 μm shows the maximum.*

    We have added text at the end of Section 5 about the comparison with SPC measurements from the literature (p.19-22).

15. *Page 13, line 18; In accordance with the procedures newly introduced in this manuscript, MASC images are classified and results are shown in Figures 9 and 10, and Table 3. Are they reasonable and are there any specific features derived with this analysis? Have you got any new findings? In other words, what sort of contributions you could achieve to the geophysical and cryospherical research field? Or, you would like to remain in just the introduction of the methodology?*

    The primary goal of this manuscript is to introduce the proposed methodology to derive information about blowing snow from the MASC. We provide illustration from two contrasted data sets (Alps vs Antarctica) in order to evaluate if the outcome makes sense (and it does!). We also compare the obtained statistics on blowing-snow particle size to reference information from the literature to illustrated the limitations of the proposed approach, mainly related to the too-coarse resolution of the MASC to fully capture the entire size range of blowing snow. This is now clearly mentioned in the text (end of Section 5 and 6).

16. *Figures 6 and 8: No explanations were found in the text. Further, in general, descriptions about the figure are rather brief both in figure captions and text. More detailed explanation is recommended, that will be help to deepen the understandings.*

    We have added text in Sections 4 and 5 to better describe these figures and their analyses.

Identification of blowing snow particles in images from a multi-angle snowflake camera

Mathieu Schaer[1], Christophe Praz[1], and Alexis Berne[1]

[1] Environmental Remote Sensing Laboratory, École Polytechnique Fé dérale de Lausanne, Switzerland

Correspondence: Alexis Berne (alexis.berne@epfl.ch)

Abstract. A new method to automatically discriminate between hydrometeors and blowing snow particles on Multi-Angle Snowflake Camera (MASC) images is introduced. The method uses four selected descriptors related to the image frequency, the number of particles detected per image as well as their size and geometry to classify each individual image. The classification task is achieved with a two components Gaussian Mixture Model fitted on a subset of representative images of each class from field campaigns in Antarctica and Davos, Switzerland. The performance is evaluated by labelling the subset of images on which the model was fitted. An overall accuracy and Cohen's Kappa score of 99.4 and 98.8%, respectively, is achieved. In a second step, the probabilistic information is used to flag images composed of a mix of blowing snow particles and hydrometeors, which turns out to occur frequently. The percentage of images belonging to each class from an entire austral summer in ~~Antartica~~ Antarctica and during a winter in Davos, respectively, are presented. The capability to distinguish precipitation, blowing snow and a mix of those in MASC images is highly relevant to disentangle the complex interactions between wind, snowflakes and snowpack close to the surface.

1 Introduction

Over snow covered regions, ice particles can be lifted from the surface by the wind and suspended in the atmosphere. Wind-driven snow transport is ubiquitous in the cryosphere: over complex terrain (e.g. Winstral et al., 2002; Mott and Lehning, 2010), over ~~toundra~~tundra/prairies (e.g. Pomeroy and Li, 2000) and over polar ice sheets (e.g. Bintanja, 2001; Déry and Yau, 2002; Palm et al., 2011). Wind-driven snow transport must be taken into account to obtain accurate estimates of the mass balance and radiative forcings at the surface (e.g. Gallée et al., 2001; Lesins et al., 2009; Scarchilli et al., 2010; Yang et al., 2014). In mountainous regions, wind-transported snow also creates local accumulations and irregular deposits, being a critical factor influencing avalanche formation (e.g. Schweizer et al., 2003). Quantifying snow transport during snowfall events and subsequent periods of strong winds is essential for local avalanche prediction (e.g. Lehning and Fierz, 2008). In the context of climate change, the mass balance of the Antarctic ice sheet is of increasing relevance due to its impact on sea level rise (Shepherd et al., 2012). The sustained katabatic winds in Antarctica generate frequent blowing snow events, that remove a significant amount of new snow through transport and sublimation. Wind-transported snow is hence an important factor to take into account when considering Antarctic mass balance (e.g. Déry and Yau, 2002; Scarchilli et al., 2010; Lenaerts and van den Broeke, 2012; Das et al., 2013). Blowing snow is also an important process for the mass balance of the Greenland ice sheet (e.g. Box et al., 2006).

The layers formed by wind-suspended ice particles are commonly separated in two classes: drifting snow when the top of this layer is less than ~~2 m~~ 2 m above ground, blowing snow above (see http://glossary.ametsoc.org for instance). The present study focuses on blowing snow because the observations used for detection were collected more than ~~2 m~~ 2 m above ground (but the proposed approach could easily be extended to drifting snow if relevant data are collected/available).

Blowing snow is challenging to measure and characterize. Various approaches have been proposed to monitor blowing snow at ground level: mechanical traps, nets, photoelectric or acoustic sensors, photographic systems (see Leonard et al., 2012, for a more detailed review). Although not specifically designed for blowing snow, present weather sensors have been shown to be valuable to monitor drifting and blowing snow fluxes (e.g. Bellot et al., 2011). Remote sensing, and lidar systems in particular, have recently been used to characterize the occurrence and depth of blowing snow layers, either from space ~~Palm et al. (2011)~~ (Palm et al., 2011) or near ground-level ~~Gossart et al. (2017)~~(Gossart et al., 2017). Suspended ice particles are under the influence of the gravitational force, proportional to the size cubed while the drag force is proportional to the area (size squared). With a greater area to mass ratio, smaller particles are thus more likely to be lifted in the suspension layer. A comparison of ten different studies of measured and simulated particle size distributions of blowing snow, reveals mean diameters at heights above $0.2\,\mathrm{m}$ ranging from 50 to $160\,\mu\mathrm{m}$ (Gordon and Taylor, 2009).

Blowing snow may also contaminate precipitation observations collected by ground-based sensors, obviously in Antarctica ~~(e.g. Gossart et al., 2017)~~ (e.g. Nishimura and Nemoto, 2005; Gossart et al., 2017) where winds are strong and frequent, but also in snowy regions in general ~~(Rasmussen et al., 2012; Scaff et al., 2015)~~(Rasmussen et al., 2012; Naaim-Bouvet et al., 2014; Scaff et al . The issue of snowfall measurement is complex and WMO promoted intercomparison projects to evaluate various sensors and define standards set-ups and protocols over the last two decades, as illustrated in (Goodison et al., 1998) and the recent SPICE project (http://www.wmo.int/pages/prog/www/IMOP/intercomparisons/SPICE/SPICE.html).

The Multi-Angle Snowflake Camera (MASC) is a ground-based instrument designed to automatically captures high resolution ($\sim$33.5 μm) photographs of falling hydrometeors from three different angles (Garrett et al., 2012). The MASC has been used in ~~prevuous~~ previous studies to investigate snowflake properties (Garrett et al., 2015; Grazioli et al., 2017) and to help interpret weather radar measurements (Kennedy et al., 2018). Interestingly, blowing snow particles also trigger the motion detector system, producing many images in windy environments. Combined with the hydrometeor classification techniques based on MASC images (e.g. Praz et al., 2017), the ability to discriminate between images composed of blowing snow and precipitation particles is therefore relevant to characterize blowing snow, to provide reference observations to improve its remote sensing, as well as to obtain more accurate snowfall estimates from ground-based sensors. More generally, detailed information about the type of particles pictured by a MASC will enable us to further investigate the complex interactions between wind, snowflakes and snowpack close to the surface in cold and windy regions.

This article presents a new method to automatically determine if an image from the MASC (and potentially other imaging instruments) is composed of blowing snow particles, precipitating hydrometeors (snowflakes and ice crystals) or a mix of both.

The classification is accomplished by means of a Gaussian mixture model (GMM) with two components, fitted on a set of representative MASC images and evaluated on a manually-built validation set. The paper is organized as follows: Section 2 introduces the data sets used to develop the method and fit the GMM. Section 3 illustrates the different steps to isolate the particles and extract related features for the clustering task. Section 4 explains the selection of the most relevant features, the fitting of the GMM as well as the attribution of a flag for mixed images. The main results are shown in Section 5. At last, limitations and further improvements are discussed in Section 6.

2 ~~Data~~ Instrument and data sets

2.1 The Multi-Angle Snowflake Camera

The MASC is a ground-based instrument which automatically takes high-resolution and stereoscopic photographs of hydrometeors in free fall while measuring their fall velocity. Its working mechanism is only summarized hereafter, as more details and explanations can be found in Garrett et al. (2012), who provide an extensive description of the instrument. Three high-resolution cameras (2448×2048 pixels), separated by an angle of 36°, are attached to a ring structure and form altogether the imaging unit (see Fig. 1). The focal point is located inside the ring at about 10 cm from each camera. Particles falling through the ring and detected by the two horizontally aligned near-infrared emitter-receiver arrays trigger the three flashes and the three cameras. The cameras' apertures and exposure times were adjusted in order to maximize the contrast on hydrometeor photographs while preventing motion blur effects, leading to a resolution of about 33.5 µm and a sampling area of about 8.3 cm^2 (see Praz et al., 2017). The maximum frequency of triggering is 3 Hz, that is three image triplets per second.

Figure 1. Left: side-view of the MASC with the three flash lamps in white on top, the two detectors as white boxes on the side of the metal ring (in black and red in front). Right: top view of the inside of the MASC, with the three cameras clearly visible.

These specifications can be compared to the snow particle counter (SPC) which has been used in many studies of blowing snow (e.g. Nishimura and Nemoto, 2005; Gordon and Taylor, 2009; Guyomarc'h et al., 2019) and can be considered as the reference

Figure 2. Experimental set-up conditions of the MASC in a DFIR near Davos (left) and on top of a container at ~~DDU~~ Dumont d'Urville (right).

instrument for monitoring blowing snow (e.g. Crivelli et al., 2016). The SPC has a control volume of $2 \times 25 \times 0.5\,\mathrm{mm}^3$ and assigns particles into 32 diameter classes between 50 and $500\,\mu\mathrm{m}$. It provides information on particle diameter (assuming a spherical shape), particle number and particle mass flux at a 1-s resolution. For more information about the SPC, the reader is referred to the articles mentioned above.

2.2 Data sets

The MASC data used to implement and validate the present algorithm were collected during three field campaigns. The first one took place in Davos, Switzerland during the winter 2015-2016. The MASC was placed at $2540\,\mathrm{m}$ a.s.l in a Double Fence Intercomparison Reference (DFIR, see Fig. 2, left), designed to limit the adverse effect of wind on the measuring instruments in its center (Goodison et al., 1998). The MASC was about $3\,\mathrm{m}$ above ground. The two other campaigns took place at the French Antarctic Dumont d'Urville station, on the coast of Adelie Land, during the austral summer 2015-2016 and from January to July 2017 in the framework of the Antarctic Precipitation, Remote Sensing from Surface and Space project[1](Grazioli et al., 2017; Genthon et al., 2018). The instrument was deployed on a rooftop at about $3\,\mathrm{m}$ above ground (see Fig. 2, right). A collocated weather station and a micro rain radar (MRR) were also installed. Nearly three millions images were collected during these measurement campaigns all together.

From this great amount of data, subsets of pure precipitation and pure blowing snow images were manually selected and further analyzed to chose relevant descriptors and fit a two components GMM. The task of selecting enough representative images from both class appeared less trivial than expected, especially for Antarctica, as mixed images are especially common. Gossart et al. (2017) used ceilometer data collected at the Neumayer and Princess Elizabeth stations in East Antarctica to investigate blowing snow, and they suggests that more than 90% of blowing snow occurs during synoptic events, usually

[1] http://apres3.osug.fr

Table 1. Campaigns and dates of selected events for the Blowing snow (BS) and Precipitation (P) subsets.

Antarctica 15-16	Antarctica 17	Davos 15-16
11 Nov BS	08 Feb BS	23 Feb P
22 Nov P	09 Feb BS	25 Feb P
15 Dec P	18 Feb BS	04 Mar P
16 Dec P	19 Feb BS	05 Mar P
30 Dec P		16 Mar P
02 Jan P		25 Mar P
11 Jan P		
28 Jan BS		

combined with precipitation. For the sake of generalization, as many representative events as possible were selected across the three campaigns. The goal was to cover a wide range of hydrometeors types as well as snowfall rate for the precipitation subset. Similarly, varying wind speeds and concentration densities were considered to build the blowing snow subset. From the campaigns in Antarctica, pure blowing snow and hydrometeors events were highlighted by comparing time series of MASC image frequency, wind speed and MRR derived rain rate, as illustrated in Figure 3. It was noticed that during strong blowing snow events, the number of images captured by the MASC was ~~exceptionally important~~much larger than during precipitation events (more than 1 image per second, see Fig. 6). Potential pure blowing snow events were selected when the MASC image frequency and wind speed were higher than their respective median observed over the whole campaign and no precipitation was detected during the preceding hour. Only events for which these criteria applied for over an hour consecutively were kept. To highlight pure precipitation, the principle was the same but the criteria were an image frequency and a wind speed lower than the median and a MRR precipitation rate greater than zero. The MRR has a certain detection limit, so it was noticed that events selected as blowing snow could also occur during undetected light precipitation. As a result, images from all events were rapidly checked ~~vizually~~ visually and the campaign logbook consulted to ensure that the selection was consistent and coherent. In both cases, some events had to be removed because of obvious mixing of blowing snow and hydrometeors.

As the MASC was deployed inside a DFIR in Davos, no blowing snow events were selected from this campaign. Although the DFIR is supposed to shelter the inner instruments from wind disturbances, we noticed that many images do not solely contain pure hydrometeors. From a webcam monitoring the instrumental set up, one could notice that the fresh snow accumulated on the edges and borders of the wooden structure of the DFIR was frequently blown away towards the sensor. To augment the precipitation subset, events with high snowfall rate but not affected by outliers of fresh wind-blown snow were added. Finally, some sparse images of obvious pure hydrometeor in the middle of mixed events were also included in the training set. In total, each subset contained 4263 images and despite possible remaining (limited) uncertainty in the exact type of images, is assumed to be accurate and reliable enough to serve as reference for the evaluation of the proposed technique (see Fig. 8 and Section 4.2).

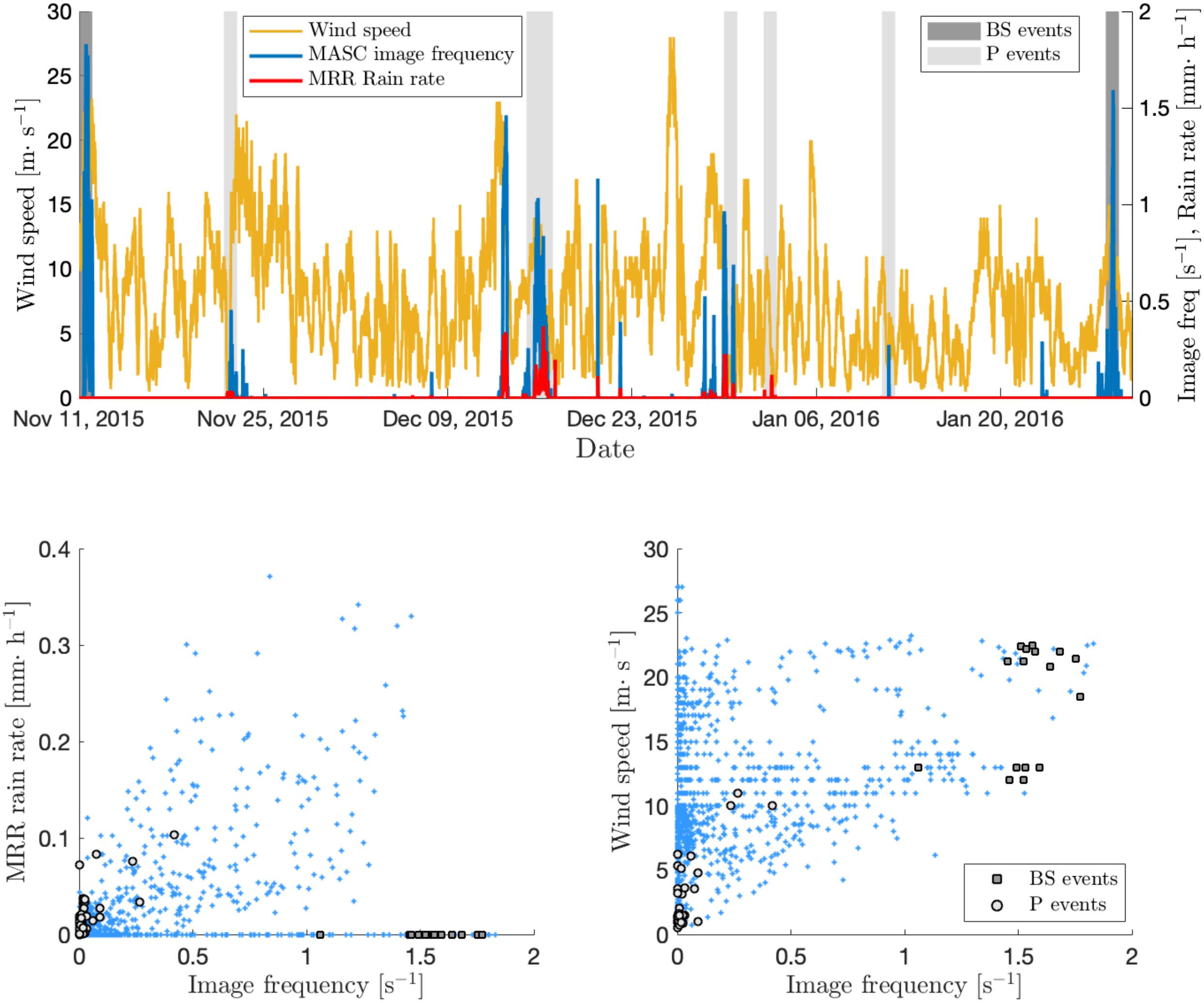

Figure 3. Time series and scatter plots of MASC image frequency, wind speed (measured at 10 m) and MRR derived rain rate for the Antarctica 2015-2016 campaign. The grey shading indicates days during which time steps have been selected for the training set as blowing snow (dark grey) or precipitation (light grey). In the bottom scatter plots, the markers figure the selected blowing snow and precipitation time steps. Points on the x-axis in the left scatter plot are potential candidates for pure blowing snow.

3 Image Processing

3.1 ~~Particles~~ Particle detection

The MASC consists of three cameras mounted on a ring structure with an angle of 36° between them and sharing the same focal point in the middle of the ring. The motion detector system is composed of two horizontally aligned near-infrared emitter-receiver arrays, which delimit a $8.3\,\mathrm{cm}^2$ detection surface in the center of the structure, where the two beams overlap (see Garrett et al., 2012, for more details). A particle passing through this area triggers the cameras together with three spotlights that illuminate the target. In the present study, all images have a size of 2448×2048 pixels.

Although a single particle activates the cameras, many MASC pictures contain multiple particles distributed over the entire image, especially when blowing snow occurs. In fact, the number of particles appearing on a single image is a key characteristic to distinguish between precipitation and blowing snow. As a result, it was deemed essential to detect all particles in each image rather than the triggering one only (which is sometimes unidentifiable). A key challenge of this approach was to get rid of the noisy background. For this purpose, a median filter was used. The brightness of the background strongly depends on the luminosity at the instant of the picture, which varies according to the time of day and can change abruptly in partly cloudy conditions when the sun suddenly appears from behind a cloud. As a result, the median filter shows better performance to remove the background when systematically re-computed over a small number of consecutive images. Assuming that snow particles hardly appear at the exact same position on few consecutive images, the median filter was chosen to be computed over blocks of 5 images per camera angle. To ensure complete removal of the background when its brightness is greater that the corresponding median, a factor of 1.1 was applied to the filter. Finally, as some limited residual noise can still remain in the filtered image, a small detection threshold of 0.02 grayscale intensity was applied to isolate the snow particles. Masks of the sky and reflecting parts of the background (i.e. metallic plates etc) were created for each camera. The multiplication factor and detection threshold are increased in the regions delineated by the masks if the normal filtering leads locally to more pixels detected that one can expect from real particles. These steps are illustrated in Figures 4 and 5. Issues in the filtering may occur if consecutive images are separated by a too long period of time, during which the ambient luminosity has changed significantly (e.g. before/after the sunrise or sunset). An example is shown in Figure B1 in Appendix B.

3.2 Feature extraction

Machine learning algorithms require a set of variables, commonly called features or descriptors, upon which the classification is performed. Because of the fragmentation of ice crystals when hitting the ground surface (e.g. Comola et al., 2017), blowing snow is expected to be characterized by much smaller particle size and much higher particle concentration than snowfall (e.g. Nishimura and Nemoto, 2005; Naaim-Bouvet et al., 2014). In this study, various quantitative descriptors were therefore calculated according to four different categories: the number of particles and their spread across the image, the size of the particles, the geometry of the particles and the frequency at which the images are taken.

Since it is difficult to exactly guess which descriptors are the most adequate to differentiate between blowing snow and precipitation images, an extensive collection of features was extracted from the blowing snow and precipitation subsets and

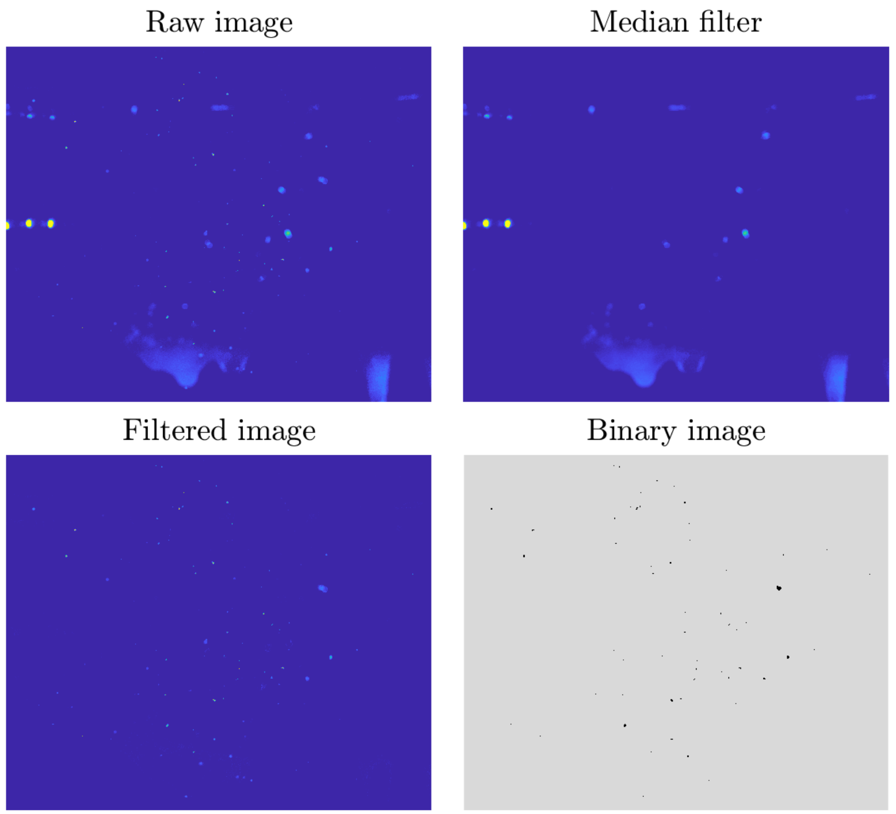

Figure 4. Raw image, median filter, filtered image and final binary image for an example of blowing snow particles. The image size is 2448×2048 pixels, corresponding to $82 \times 68.6\,\mathrm{mm}^2$. Original MASC images are in grey shades, but the color scheme ~~is~~ used here aims to enhance contrast and details for visual purposes.

compared. The selection of the most relevant ones is explained in the next section. As the classification is performed at the image level, the information on the geometry and size of each detected particle in the image was transformed into a single descriptor. Consequently, quantiles ranging from 0 to 1 and moments from 1 to 10 were computed out of the distribution of the considered feature within the image. The image frequency is a descriptor independent from the content of the image and thus from the detection of particles. It is therefore not affected by potential image processing issues. As each image comes with its attributed timestamp, the average number of images per minute was calculated with a moving window. The full list of all computed descriptors is displayed in Appendix A. The extraction of features was conducted with the `MATLAB` Image Processing Toolbox, in particular the function `regionprops`[2].

[2]https://ch.mathworks.com/help/images/ref/regionprops.html

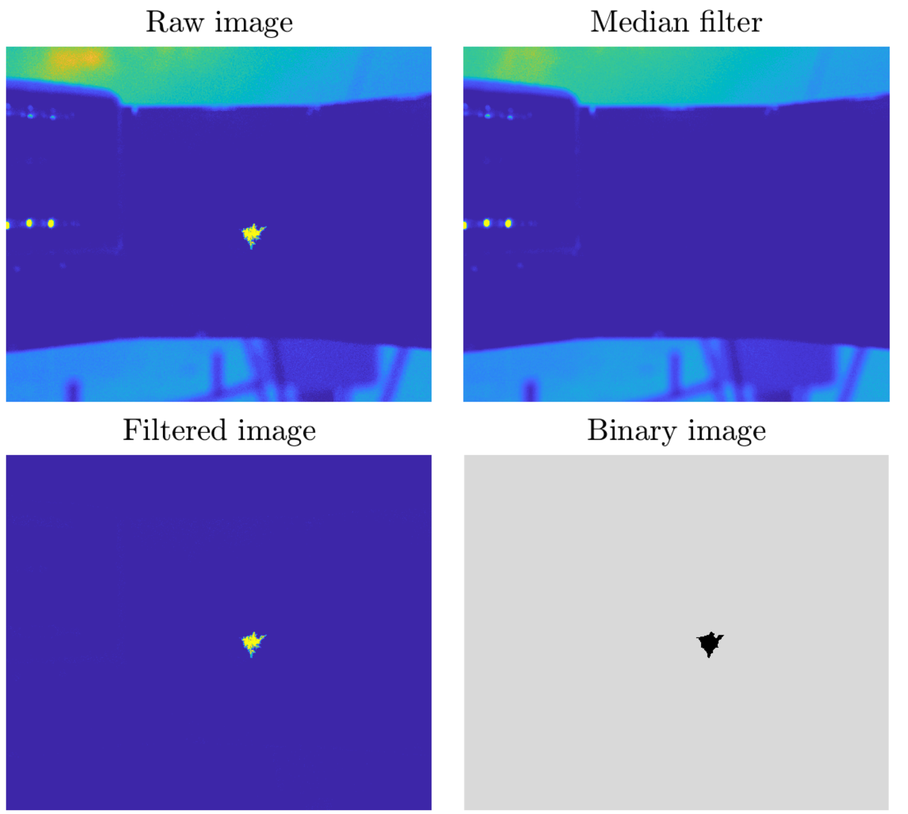

Figure 5. Raw image, median filter, filtered image and final binary image for an example of hydrometeor. The color scheme is used to enhance details for visual purposes.

4 Classification

4.1 Feature selection and transformation

Selecting a pertinent set of features and avoiding redundancy is essential for accurate classification, regardless of the classification algorithm. For each of the four categories of descriptors previously mentioned, the most relevant one (according to the criterion explained below) was kept. The descriptor maximizing the “inter-clusters over intra-clusters" distance described in Eq. 1 was selected. This quantity represents the distance between the mean of the blowing snow and precipitation distributions (μ_{BS} and μ_P respectively), normalized by the sum of their respective standard deviations (σ_{BS} and σ_P respectively).

$$S = \frac{|\mu_{BS} - \mu_P|}{\frac{1}{2}(\sigma_{BS} + \sigma_P)}. \quad (1)$$

Table 2. Selected features and corresponding S values

Feature name	S
Image frequency	4.43
Cumulative distance transform	2.89
Maximum diameter quantile 0.7	1.71
Squared fractal index quantile 0	3.81

For the features describing the number of detected particles and their spread across the image, the *cumulative distance transform* was kept. It represents the sum over each entry of the distance transform matrix[3]of the binary image. The distance transform matrix has the same dimensions as the binary image and computes, for each pixel, the Euclidean distance to the nearest 1 element (i.e. the nearest particle). As a result, an image with many particles well distributed over its entire surface will have a low *cumulative distance transform*, while a single particle, even particularly large, will have a high value. This descriptor is more robust to image processing issues than the raw number of particles, as illustrated in Figure B2 in Appendix B.

Concerning the size distribution of the particles detected in an image, the quantile 0.7 of the maximum diameter was selected. The maximum diameter (*Dmax*) represents the longest segment between two edges of a particle (see Praz et al., 2017, for more details). A logarithmic transformation of this feature was performed to make the distributions of the two classes more Gaussian. The minimum (i.e. quantile 0) squared fractal index showed the greatest S value (hence discrimination potential) among the features related to the particle geometry indices. The fractal index (FRAC) is defined according to the formula proposed by McGarigal and Marks (1995) in the context of ~~landscape pattern~~ landscape-pattern analysis. It was also more recently used to quantify stand structural complexity from terrestrial laser scans of forests (Ehbrecht et al., 2017).

Due to its different nature, the image frequency descriptor was selected by default, but it is worth noting that it has the highest S value (Eq. 1) among all descriptors (Table 2). The marginal distributions of the selected descriptors for the training set are shown in Figure 6 to provide an idea of their respective magnitude and variability, as well as to illustrate their discrimination potential. As noted above, the image frequency is the most informative descriptor to distinguish blowing snow and precipitation.

In summary, four descriptor categories (related to particle size, particle geometry and particle distribution within the image as well as image frequency) have been defined to distinguish images collected during blowing snow or snowfall, based on the expected differences in particle size and concentration between the two. A number of descriptors were estimated from each image by computing various quantiles and moments of the distributions of geometric properties of the particles in the considered image. One descriptor from each of the four categories defined above (listed in Table 2) was then selected to be further used for classification as the one maximizing the “inter-clusters over intra-clusters" distance defined in Eq. 1.

[3]https://ch.mathworks.com/help/images/ref/bwdist.html

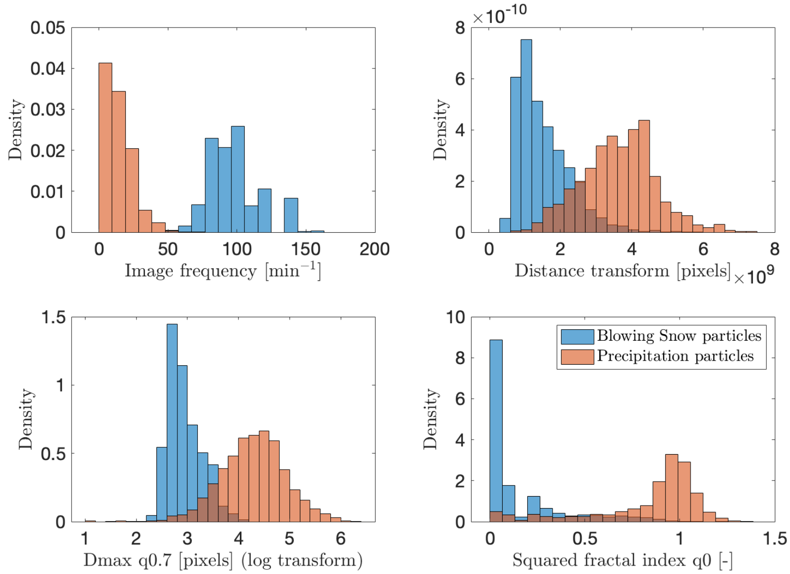

Figure 6. Histograms of selected descriptors for the training blowing snow and precipitation subsets.

4.2 Model fitting

The choice for the binary classification task was made on a Gaussian mixture model, an unsupervised learning technique that fits a mixture of multivariate Gaussian distributions to the data (see Murphy, 2012; McLachlan and Basford, 1988; Moerland, 2000, for more details). The mathematical description of a multivariate normal distribution is provided in Eq. 2.

$$\mathcal{N}(\boldsymbol{x}|\boldsymbol{\mu},\boldsymbol{\Sigma}) = \frac{1}{(2\pi)^{D/2}|\boldsymbol{\Sigma}|^{1/2}} \exp\{-\frac{1}{2}(\boldsymbol{x}-\boldsymbol{\mu})^T\boldsymbol{\Sigma}^{-1}(\boldsymbol{x}-\boldsymbol{\mu})\}. \tag{2}$$

where $\boldsymbol{x}$ is a multivariate random variable of dimension D, $\boldsymbol{\mu}$ its mean and $\boldsymbol{\Sigma}$ its covariance matrix, with ^{T} the transpose operator.

The justification for the unsupervised approach is manifold. First, unsupervised methods do not depend upon labels. Hence, it is not required to ensure correct labelling of each image in the training set. As mentioned earlier, many images are composed of mix of blowing snow and precipitation and it is thus difficult to guarantee the objectivity of all given labels. Second, a clear separation observed between the two subsets would be statistically highly significant as no prior information is provided to the learning algorithm about the classes. Third, for low dimensional problems, unsupervised methods are sometimes less prone to over-fitting and have a better potential of generalization. A main advantage of the GMM compared to other unsupervised methods is to provide posterior probabilities on the cluster assignments and thus allow for soft clustering (i.e. probabilistic assignment). In the context of the present study, this is absolutely relevant as there exists a whole continuum of in-between cases of mixed images. It should be noted that the descriptors were selected using a reference set (see previous section), but the clustering conducted by means of the GMM is itself unsupervised.

$$\mathcal{N}(x|\mu,\Sigma)=\frac{1}{(2\pi)^{D/2}|\Sigma|^{1/2}}\exp\{-\frac{1}{2}(x-\mu)^T\Sigma^{-1}(x-\mu)\}.$$

A two components GMM with unshared full covariance matrices was thus fitted to the four dimensional data composed of the blowing snow and precipitation subsets. The `MATLAB` Statistics and Machine Learning Toolbox was used to this purpose and the model parameters were estimated by maximum likelihood via the Expectation-Maximization (EM) algorithm[4]. The features were standardized before fitting the model. The mixing weights (or component proportions) were artificially set to 0.5 by randomly removing 80 data points from the training set and fitting again the GMM to have perfectly balanced classes. This step is essential as the model will then be used to classify new images (possibly from other campaigns). There are no reasons to give more weight to one component, as the relative proportion of blowing snow and precipitation images strongly depends on the campaign location. The posterior probabilities are computed using Bayes rule (Murphy, 2012):

$$P(z_i=k|\boldsymbol{x}_i,\boldsymbol{\theta})=\frac{P(\boldsymbol{x}_i|z_i=k,\boldsymbol{\theta})P(z_i=k|\boldsymbol{\theta})}{P(\boldsymbol{x}_i|\boldsymbol{\theta})}, \tag{3}$$

where z_i is a discrete latent variable taking the values $1,...,K$ and labelling the K Gaussian components. $P(z_i=k|\boldsymbol{x}_i,\boldsymbol{\theta})$ is the posterior probability that point i belongs to cluster k (also known as the "responsibility" of cluster k for point i). $P(\boldsymbol{x}_i|z_i=k,\boldsymbol{\theta})$ corresponds to the density of component k at point i (i.e. $\mathcal{N}(\boldsymbol{x}_i|\boldsymbol{\mu}_k,\boldsymbol{\Sigma}_k)$) and $P(z_i=k|\boldsymbol{\theta})$ represents the mixing weight (also denoted π_k). Note that the π_k are positive and sum to 1. $\boldsymbol{\theta}$ refers to the fitted parameters of the mixture model $\{\boldsymbol{\mu}_1,...,\boldsymbol{\mu}_k,\boldsymbol{\Sigma}_1,...,\boldsymbol{\Sigma}_K,\pi_1,...,\pi_K\}$. $P(\boldsymbol{x}_i|\boldsymbol{\theta})$ is the marginal probability at point i, which is simply the weighted sum of all component densities:

$$P(\boldsymbol{x}_i|\boldsymbol{\theta})=\sum_{k=1}^{K}\pi_k\mathcal{N}(\boldsymbol{x}_i|\boldsymbol{\mu}_k,\boldsymbol{\Sigma}_k). \tag{4}$$

As the concern of this study is on two components only, a more compact notation will be used for the rest of the article. The latent variable z will be replaced by k_P and k_{BS} to refer to the precipitation and blowing snow clusters, respectively. The term $\boldsymbol{\theta}$, that denotes the model parameters, will be left implicit. Assuming we are at first interested by performing some hard clustering (i.e. single label to a given image), an image will be classified as blowing snow if $P(k_{BS}|\boldsymbol{x}_i)>P(k_P|\boldsymbol{x}_i)$. In words, if the posterior probability to belong to the blowing snow cluster is greater than 0.5, an image will be classified as such (because the posterior probabilities sum to 1). The model performance was assessed by simply labelling the data points according to its initial subset. An overall accuracy of 99.4% and a Cohen's Kappa score of 98.8% were achieved. The Cohen's Kappa statistic adjusts the accuracy by accounting for correct predictions occurring by chance (Byrt et al., 1993). These high values indicate a very good performance of the fitted GMM. Figure 7 presents the fitted Gaussian components as well as the reference values (not used in the fitting) for each of the 6 possible pairs of the 4 descriptors. It clearly illustrates the performance of the fitted GMM and the discriminative power of the descriptor related to image frequency.

[4] https://ch.mathworks.com/help/stats/gaussian-mixture-models-2.html

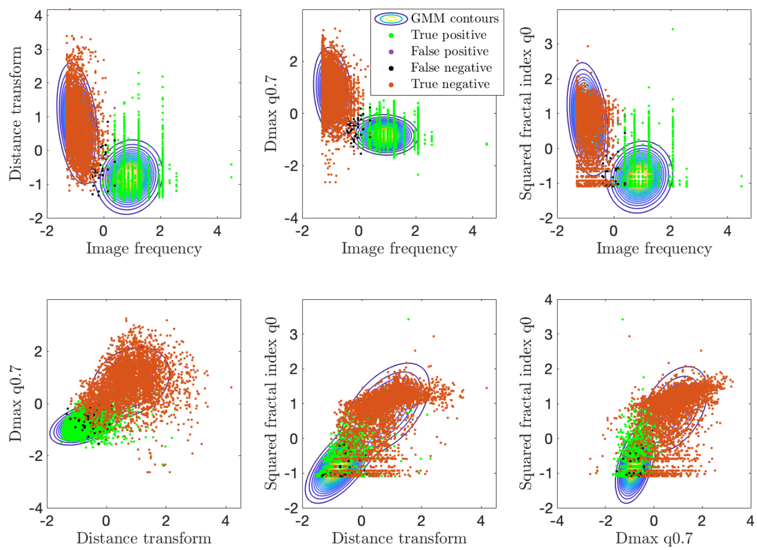

Figure 7. GMM contours and data points projected on the 2D planes. The colors correspond to the four entries of the confusion matrix. The predictions result from the clustering and the ground truth is the given labels.

To investigate the stability of the Gaussian components, the precipitation and blowing snow subsets were both randomly permuted and divided in ten equal parts. Ten new training sets of balanced amount of each subset were created and new GMM fitted. Figure 8 shows on the top line the boxplots of the Gaussian components parameters $\boldsymbol{\mu}_d$ and $\boldsymbol{\sigma}_d$ (i.e. diagonal entries of $\boldsymbol{\Sigma}$) for each of the four dimensions. The boxplots show a limited variability for each feature (below 10%), indicating a reasonable stability of the fitted parameters. In addition, the bottom line of Figure 8 presents the learning curves, and their fast convergence to the same horizontal line when more than 30% of the training set is used, indicates a ~~training~~ data set large enough for a reliable fitting of the GMM, without overfitting.

4.3 Flag for mixed images

As mentioned earlier, an asset of using a GMM model is the posterior probabilistic information that could help estimate the degree of mixing of an image. Data points located close to the decision boundary in the multidimensional space are likely to be composed of a mix of blowing snow particles and hydrometeors. However, distributions of posterior probabilities computed over thousands of new images from entire campaigns, showed that they were stretched out on both end of the domain (i.e. close to 0 or 1) and not many images were present in between. This is probably due to the nature of the descriptors and the resulting shapes and relative positions of the Gaussian distributions. Nevertheless, a subset of mixed images, specially created for this purpose, highlighted clear discrepancies on the posterior probabilities with the pure blowing snow and precipitation subsets. However, this differentiation was around 10^{-6} (or $1-10^{-6}$), which is not so informative as such. Consequently, it was

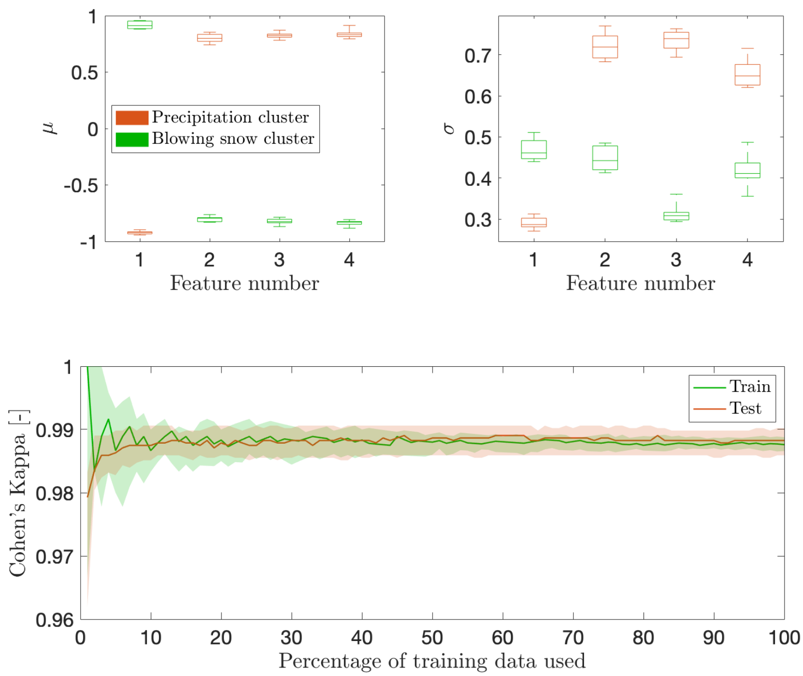

Figure 8. Top: stability of the parameters μ and σ (diagonal entries of $\boldsymbol{\Sigma}$) for the two Gaussian components. The boxplots show the distributions of these parameters for each dimension, after fitting the GMM on a 10-fold random split of the training set. The feature number follows the order given in Table 2. Bottom: learning curves for the fitted GMM, showing the evolution of the train and test Cohen's kappa as a function of the proportion of the training samples used. The shaded areas correspond to the 25–75 percentile range computed over 40 iterations of 70-30% random train-test splitting and bold lines are the medians.

decided to define a new index, similar to the posterior probability to belong to the blowing snow component, but more evenly distributed across the range $]0,1[$. The new index uses the negative logarithm of the posterior probabilities multiplied by the marginal probability. Taking the log of Eq.3 for k_{BS}, we have (the same applies for k_P):

$$-\log[P(k_{BS}|\boldsymbol{x}_i)P(\boldsymbol{x}_i)] = -\log[P(\boldsymbol{x}_i|k_{BS})P(k_{BS})]. \tag{5}$$

Noting that the term $P(\boldsymbol{x}_i|k_{BS})$ on the right hand side is $\mathcal{N}(\boldsymbol{x}_i|\boldsymbol{\mu}_{BS},\boldsymbol{\Sigma}_{BS})$, one can substitute Eq. 2 into the above expression, which yields:

$$-\log[P(k_{BS}|\boldsymbol{x}_i)] - \log[P(\boldsymbol{x}_i)] = \frac{1}{2}(\boldsymbol{x}_i - \mu_{BS})^T \Sigma\boldsymbol{\Sigma}_{BS}^{-1}(\boldsymbol{x}_i - \mu_{BS}) + \frac{1}{2}\log(|\Sigma\boldsymbol{\Sigma}_{BS}|) + \frac{D}{2}\log(2\pi) - \log(P(k_{BS})). \tag{6}$$

The quadratic term on the right hand side is the Mahalanobis Distance, which is a distance that uses a Σ^{-1} norm. Hence, it represents the distance between point $\boldsymbol{x}_i$ and the center of the distribution, corrected for correlations and unequal variances in the ~~features~~ feature space (De Maesschalck et al., 2000). The second term is related to the determinant of the covariance matrix and equals -3.94 for the Blowing Snow component and -2.59 for the Precipitation one. The two last terms are constant and sum to 4.37 (the component proportions were set to 0.5 and $D=4$). The right side of Eq. 6 is also known as the quadratic discriminant function (QDF, Kimura et al., 1987), commonly noted $g_k(\boldsymbol{x}_i)$. The terms have usually opposite signs, but the minus in front of the logarithm in Eq. 6 is used here to return positive values and facilitate subsequent graphical interpretations. Note that the constant term $\frac{D}{2}\log(2\pi)$ is often removed, but in this case, it ensures that $g_k(\boldsymbol{x})$ is positive, even for a Mahalanobis distance of zero. Figure 9 displays a scatter plot of the quadratic discriminant values of both components for the whole training set. The proposed index is defined as the angle of the vector representing a data point on the scatter plot, normalized by $\frac{\pi}{2}$. It is thus computed as follows:

$$\psi = \frac{2}{\pi}\arctan\left\{\frac{-\log[P(k_P|\boldsymbol{x}_i)P(\boldsymbol{x}_i)]}{-\log[P(k_{BS}|\boldsymbol{x}_i)P(\boldsymbol{x}_i)]}\right\}. \tag{7}$$

This normalized angle is bounded in $]0,1[$, with values close to 1 ~~and~~ (respectively 0) indicating a strong membership to the Blowing Snow ~~and Precipitationclusters, respectively~~(respectively Precipitation) clusters. It is closely related to the asymmetry of the Mahalanobis distances between a point $\boldsymbol{x}_i$ and the centers of the two Gaussian distributions, but corrected by the term $\frac{1}{2}\log(|\Sigma|)$ which is different for the two components. The advantage of using the index in this form, rather than deriving it from the Mahalanobis distances alone, is to respect the decision boundary given by the maximum a posteriori (MAP) rule. This means, a posterior probability of 0.5 yields a ψ index of 0.5. Finally, quantiles 0.9 ($\psi_{P0.9}$) and 0.1 ($\psi_{BS0.1}$) of the ψ index distributions of the points classified as Precipitation and Blowing Snow, respectively, are retained as thresholds to flag potential mixed images. The idea is to allow, for both classes, 10% of the training set images being flagged as mixed. This value is qualitatively supported by the distribution shown in Figure 9. It can be changed by the user to be more (increasing it) or less (decreasing it) strict on the classification as pure blowing snow or pure precipitation, depending on the intended application.

To provide the user of the method with an easily readable output, ~~an index of mixing~~ a mixing index λ_m is introduced by linearly rescaling between 0 and 1 the ψ index of the images flagged as mixed ~~. The mixed~~ (i.e. λ_m is not defined for pure precipitation or pure blowing snow images):

$$\begin{aligned}\lambda_m &= \frac{0.5}{0.5-\psi_{P0.9}}(\psi-\psi_{P0.9}) && \text{if } \psi\in(\psi_{P0.9},0.5) \\ &= \frac{0.5}{0.5-\psi_{BS0.1}}((1-\psi_{BS0.1})-\psi) && \text{if } \psi\in[0.5,\psi_{BS0.1})\end{aligned} \tag{8}$$

The mixing index also respects the hard clustering assignment boundary at 0.5~~. A mixed index > 0.5~~ : $\lambda_m > 0.5$ indicates that the image contains a mix of blowing snow and precipitation particles, but overall being closer to blowing snow and vice versa. Images with a normalized angle outside the two mixed thresholds have a NaN index of mixing and are considered as pure blowing snow particles or pure hydrometeors. Results are provided treating all images independently, but the ψ index ~~is also~~ can also be averaged among the three camera angles to provide a unique value per image identifier as well. The median of the range (max - min) covered by the ψ values from the three individual views is about 0.08 in Davos and 0.05 at Dumont d'Urville, indicating a limited variability between the three views.

In summary, the classification as mixed case is based on the angle characterizing the considered MASC image in the 2D space formed by the axis related to pure blowing snow on the one hand and the one related to pure precipitation on the other

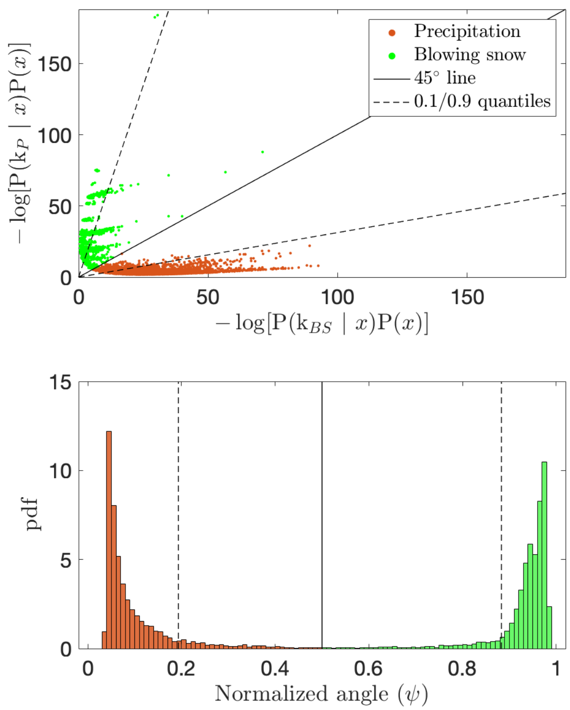

Figure 9. Top: scatter plot of the quadratic discriminant values of both components for the training set. **Bottom**: distributions of the normalized angle for the precipitation and blowing snow subsets and thresholds to identify mixed images

hand. A mixing index λ_m is finally computed by linearly rescaling the normalized angle over the range of values corresponding to mixed cases.

5 Results

The method presented in the previous sections is now tested on the entire Antarctica 17 campaign (January - July 2017) and on the entire Davos campaign (December 2015 - March 2016). About $2 \cdot 10^6$ images for Antarctica and ~~850'000~~ $8.5 \cdot 10^5$ for Davos were classified. ~~Figures 10 and 11 as well as~~ Table 3 ~~present these results. Figure 13 displays the evolution of the normalized angle for a mixed event during the Antarctica 17 campaign.~~

summarized the outcome in terms of respective proportions of pure blowing snow, pure precipitation, mixed blowing snow and mixed precipitation, for the Antarctic and Alpine data sets. As expected, the occurrence of blowing snow (pure + mixed) is much more frequent at Dumont d'Urville (75.6%) than at Davos (21.5%, out of which only 0.6% of pure blowing snow).

Figure 10 shows (top) the distribution of the collected MASC images in the space formed by the two quadratic discriminant (one for blowing snow, one for precipitation) as well as (bottom) the distribution of the normalized angle for the entire

Table 3. Percentages of MASC images per category

Class	~~Antartica~~ Antarctica (Jan - Jul 2017)	Davos (Dec 2015 - Mar 2016)
Pure Blowing snow	36.5%	0.6%
Pure Precipitation	7.2%	39.2%
Mixed Blowing snow	39.1%	20.9%
Mixed Precipitation	17.2%	39.3%

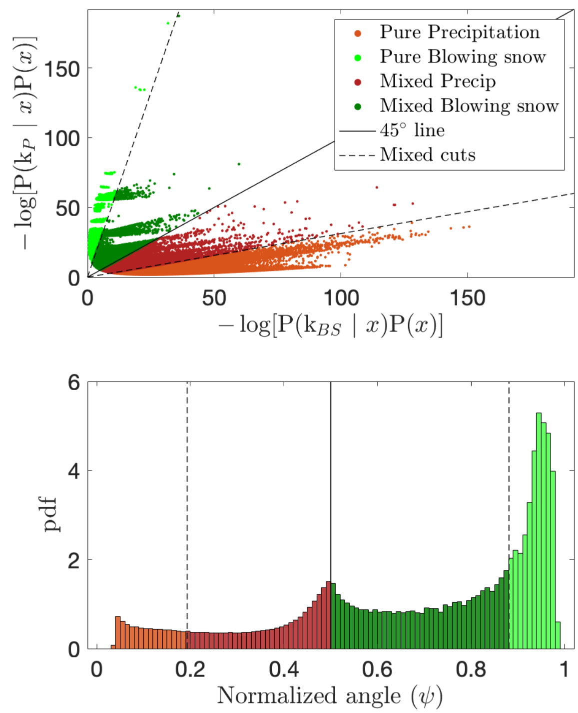

Figure 10. Top: scatter plot of the quadratic discriminant values of both components for the entire Antarctica 17 campaign. **Bottom**: distribution of the normalized angle and corresponding classification.

Antarctica 17 campaign. A clear difference with Figure 9 is the large proportion of values corresponding to mixed cases: there are much more points around the one-one line (top) and a small mode around 0.5 (bottom) for the entire campaign than for the training set (built with much less mixed cases). It is also clear from Figure 10 that blowing snow and mixed cases are dominant with respect to precipitation.

Figure 11 is similar to Figure 10 but for the entire Davos data set. In comparison with Figure 10, the occurrence of precipitation is much larger (and blowing snow much smaller), which is to be expected given the difference in geographic

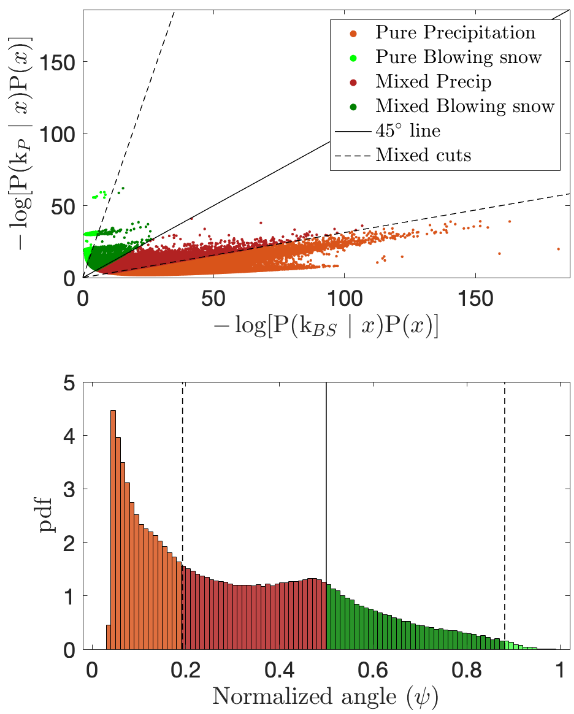

Figure 11. Same as Figure 10 for the entire Davos campaign.

context (Alps vs Antarctica) and experimental set-up (wind-protected vs no wind shield). It should be noted that mixed cases are relatively frequent and that blowing snow still happens in Davos although the MASC was located in a wind shielding fence (DFIR).

The proposed method makes also possible the analysis of the type of particles at high temporal resolution. Figure 12 shows an example of the output of the algorithm and corresponding images for a few time steps during a mixed event. It illustrates the capability of the proposed approach to distinguish blowing snow, precipitation and mixture in individual MASC images separated by a few tenths to hundredths of seconds. Over a longer time period, Figure 13 displays the evolution of the normalized angle for a mixed event during the Antarctica 17 campaign. From roughly 09:00 to 12:00, the type is dominantly precipitation and mixed, while between 12:00 and 14:00 the three types (precipitation, mixed, blowing snow) occur simultaneously. From 14:00 to 22:00, blowing snow becomes dominant (because of stronger winds). Finally, after 22:00, mixed cases dominate and some images corresponding to precipitation are even detected towards the end of the event. The possibility to identify MASC images corresponding to precipitation, blowing snow or a mixture at a temporal resolution high enough to capture the dynamics of the event is an interesting feature for regions where both are frequently associated.

~~Time series of classified MASC images and according ψ values for a mixed event during the Antarctica 17 campaign.~~

date_vec_unique	1 ID	2 Label	3 Normalized_Angle	4 Flag_mixed
25/03/2016 16:56:35	7383	1	0.7422	0.8178
25/03/2016 16:56:39	7384	0	0.1590	NaN
25/03/2016 16:56:39	7385	1	0.5659	0.5865
25/03/2016 16:56:40	7386	0	0.1437	NaN
25/03/2016 16:56:42	7387	0	0.1920	NaN
25/03/2016 16:56:42	7388	0	0.2260	0.0537

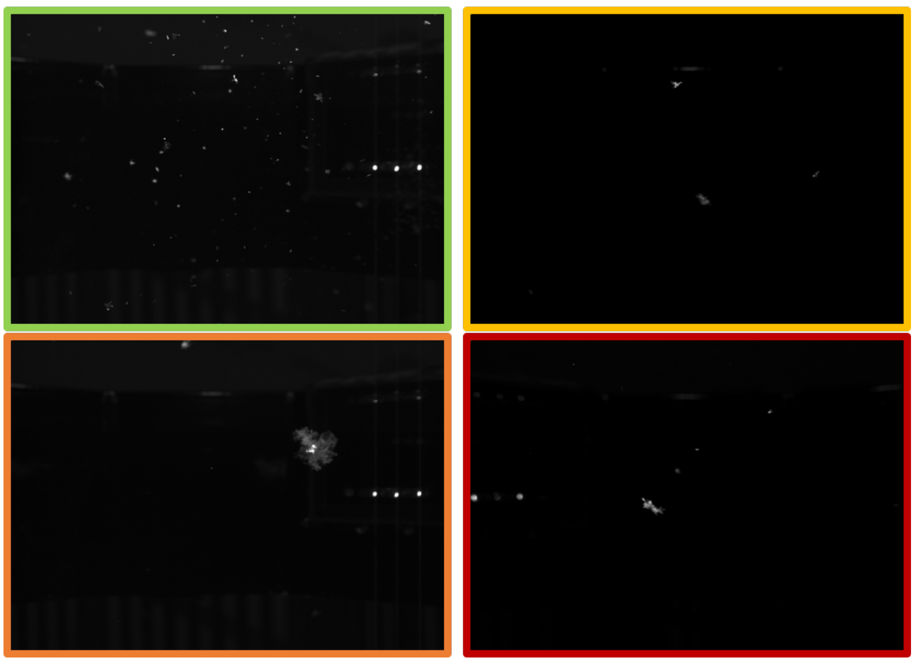

Figure 12. Consecutive MASC images from Davos and their respective classification label, normalized angle and mixing index. Label 1 is for blowing snow. A NaN mixing index means pure hydrometeor (or pure blowing snow). A mixing index close to 1 (top left image) means that it is near pure blowing snow, while a value close to 0 (bottom right image) indicate proximity to pure precipitation.

~~Histograms and fitted Gamma distributions of *Dmax* for images classified as pure blowing snow and pure hydrometeors.~~

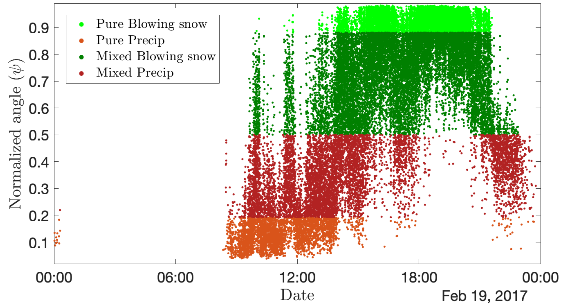

Figure 13. Time series of classified MASC images and corresponding ψ values (averaged over the three views) for a mixed event during the Antarctica 17 campaign.

~~On figure 15, an example of a potential application of the method is illustrated. Histograms and fitted Gamma distributions of *Dmax* for a large subset of~~ Considering the full Antarctic and Alpine data sets, it is interesting to analyze the potential differences in their characteristics. Figure 14 presents the distributions of the four descriptors as in Figure 6, but estimated from the entire data sets and not only the training sets (for images classified as pure blowing snow ~~and pure hydrometeors is shown. Here, the median *Dmax* in each image as been used, but all particles from each image could be taken similarly~~or pure precipitation). It can be seen that while the differences are limited for precipitation (slightly more frequent and larger in Davos than in Dumont d'Urville), they are significant for blowing snow: the blowing snow particles appear less fragmented (larger size and fractal index), less scattered within the images (larger distance transform) and with lower image frequencies in Davos. It should be recalled that the MASC was located in a wind-protecting fence in Davos, so first the occurrence of blowing snow is much smaller (0.6 vs 36.5%), and second it is likely related to fresh snow blown away from the top of the nearby fence.

The MASC resolution (33.5 µm) and thresholding (minimum 3 pixels in area) during image processing lead to an image resolution not high enough to capture in full detail the geometry of blowing snow particles. It is nevertheless interesting to plot the distribution of the measured sizes (associated with the MASC sampling area) for blowing snow and precipitation cases and compare it to existing values in the literature. Figure 15 displays the distributions of the measured size (quantified here as D_{max}) for blowing snow and precipitation in Antarctica, as well as precipitation in the Swiss Alps. To help visualize the sometimes overlapping empirical distributions, the fitted Gamma distributions are also plotted. The units are given in [mm], with the approximation that one ~~pixels~~ pixel is ~33.5 [µm]. ~~Figure~~

As expected, the size distribution of blowing snow corresponds to smaller sizes than precipitation: the mode is around 0.2 ~~12 shows an example of the output of the algorithm and corresponding images~~[mm] for blowing snow and 0.3 to 0.4 [mm] for precipitation. More importantly, the right tail of the distribution is much larger for precipitation than for blowing snow. It should also be noted that the size is slightly larger in the Alpine data set (as illustrated by the slightly larger mode of the fitted Gamma distributions).

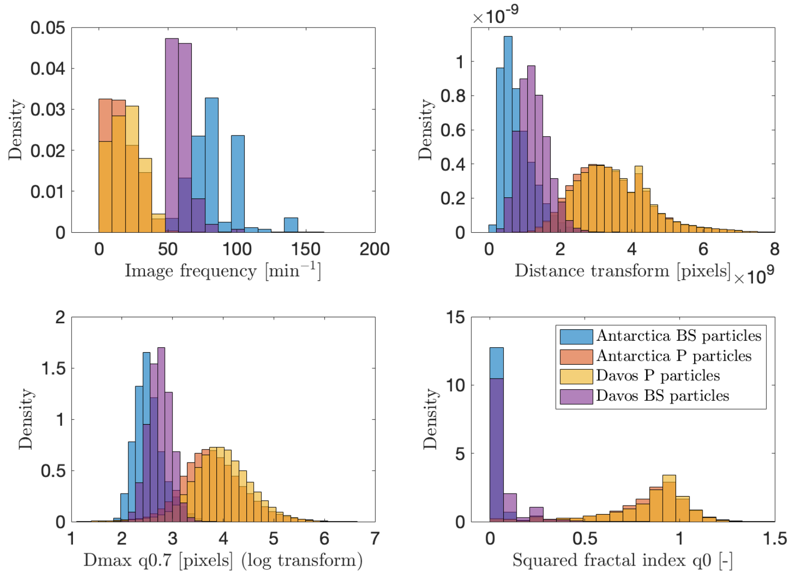

Figure 14. Histograms of selected descriptors for the training blowing snow and precipitation images from the entire Dumont d'Urville and Davos data sets.

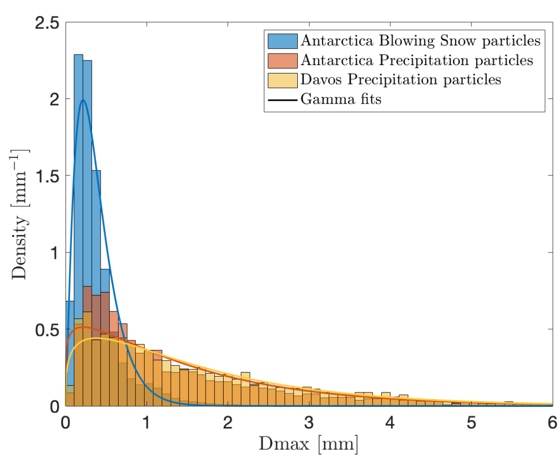

Figure 15. Histograms and fitted Gamma distributions of D_{max} for images classified as pure blowing snow and pure hydrometeors from Antarctica and pure precipitation from the Alps.

Nishimura and Nemoto (2005) provide size distributions of blowing snow and precipitation measured in Antarctica at Mizuho station using a SPC. The bimodality obtained when combining blowing snow and precipitation data in Figure 15 is in general agreement with the mixed case in their Figure 10. However, the mode for blowing snow appears at a lower size (below 50 [μm] in their Fig.7 at a height of 3.1 m). As mentioned before, this discrepancy is likely due to the limited effective resolution in MASC images after processing. In addition, as there are usually many particles in a single image during blowing snow, some may be out of focus and artificially appear larger than they are. So we expect the blowing snow features extracted from MASC data to be biased towards larger particles. It should also be noted that the sampling areas of the two instruments are different (see Section 2.1) and this could partly explain the differences in the obtained distributions.

Overall, it appears that the MASC images, processed as explained in Praz et al. (2017), are not adapted to a detailed study of the geometry of blowing snow particles, but are still relevant to distinguish blowing snow and precipitation, to characterize mixtures of both and to analyze the dynamics of blowing snow at high temporal resolutions.

~~Consecutive MASC images from Davos and their respective classification label, normalized angle and mixing index. Label 1 is for blowing snow. A NaN mixing index means pure hydrometeor (or pure blowing snow). A mixing index close to 1 (top left image) means that it is near pure blowing snow, while a value close to 0 (bottom right image) indicate proximity to pure precipitation.~~

6 Conclusions

A novel method to automatically detect images from the MASC instrument corresponding to blowing snow is introduced. The classification is achieved by a two components Gaussian mixture model fitted on a subset of 8450 representative images from field campaigns in Antarctica and Davos, Switzerland. To classify the images, the method computes four selected descriptors via image processing. The descriptors were selected to be relevant for discriminating between blowing snow particles and hydrometeors as well as to be robust to image processing artifacts. The GMM posterior probabilities are mapped into a new index that allows a better identification of mixed images and a flag signals whether an image is classified as pure hydrometeor, pure blowing snow or mixed. For mixed images, an index between 0 and 1 indicates if the image is closer to blowing snow or precipitation. The outputs are provided for each image independently or for each triplet of images (i.e. information combined over the three cameras of the MASC).

Results from a measurement campaign conducted at the Dumont d'Urville station on the coast of East Antarctica from January to July 2017 suggest that about 75% of the images are affected by blowing snow and that about 36% may be composed of blowing snow particles only (Table 3). The results also suggest that ~~57~~about 56% of the images could be made of a mix of blowing snow and precipitation particles, which support findings that in ~~Antartica~~Antarctica, blowing snow is frequently combined with precipitation ~~(Gossart et al., 2017)~~(e.g. Gossart et al., 2017). Moreover, time series of the classified images highlight that blowing snow strongly relies upon fresh snow availability and often starts shortly after the beginning of precipitation (Fig.13), which is also consistent with conclusions from Gossart et al. (2017). Results from images taken inside a Double Fence Intercomparison Reference in Davos at 2540 m a.s.l between December 2015 and March 2016, indicate that despite the sheltering structure, about 60% of the images could be affected to some extent by blowing snow particles from adjacent fence ledges. In terms of percentage of images, these numbers tend to be quite large, as the image frequency is usually much higher when strong blowing snow occurs~~. Percentages expressed~~, but the occurrence is more balanced in terms of time~~are much smaller~~.

As the method was developed and tested on fundamentally different campaigns, it may have a general applicability to any other MASC images. However, it should be noted that some descriptors depends on the particular settings (e.g. image size, pixel resolution) used during the aforementioned campaigns and a new GMM should be fitted if different settings apply. Further work should be conducted to evaluate if the method can give satisfactory results on images that do not include a timestamp, as the image frequency descriptor could not be utilized. In this case, it could be replaced by one or a couple of other descriptors listed in Table A.1 of Appendix A to strengthen the model. The method could also be adjusted to train a model with a supervised learning algorithm that provides posterior probabilities such as Bayesian classifiers or logistic regression. However, this would imply some effort to ~~improve~~ increase the training set. An inter-comparison between different machine learning algorithms and the creation of different validation sets could help gain confidence in the results.

The main limitations of the present method are the assumption of normally distributed features through the use of the GMM the too-coarse resolution of the MASC to properly capture the small end of the distribution of blowing snow particle size, and the dependency of the method on the defined training set. The latter illustrates the problem of generalization. Some extremely high intensity snowfall events, higher than the ones observed during the Davos and Antarctica campaigns, could be erroneously classified as blowing snow with the current model due to the nature of the descriptors. In this case, higher intensity pure snowfall events should be included in the training set. Another example is the size of the blowing snow particles. During the campaigns in Antarctica, the MASC was set up on a rooftop at $3\,\mathrm{m}$ a.g.l. Several studies have demonstrated that the size of blowing snow particles tends to decrease with height ~~(Nishimura et al., 2014; Nishimura and Nemoto, 2005)~~ (Nishimura and Nemoto, 2005; Nishimura et al., 2014). Consequently, blowing snow particles on images from a MASC that would have been set up at much higher or lower heights may have a bias relative to the fitted Gaussian distribution of the Blowing Snow cluster for *Dmax*. It is thus recommended to follow the procedure described in this article and fit a new model, if the one provided does not perform well in other contexts.

Appendix A: Feature extraction

Table A1. Full list of all computed descriptors. Descriptors related to each particle are transformed into a single descriptor for the image (right column). Selected ones are shown with an asterisk

Image frequency*	-
Number of particles detected in the image	-
Distance to connect all particles	-
Number of particles smaller than a given threshold	-
Ratio of the area represented by all particles to the area of the smallest polygon encircling them	-
Cumulative distance transform*	-
Maximum diameter*	quantiles 0-1, Moments 1-5
Particle area	quantiles 0-1, Moments 1-5
Particle ~~convexe~~ convex area	quantiles 0-1, Moments 1-5
Particle ~~perimiter~~ perimeter	quantiles 0-1, Moments 1-5
Fractal Index (FRAC), Fractal Index squared*	quantiles 0-1, Moments 1-5
Gravelius compactness coefficient (ratio of the perimeter to the one of a circle with equivalent area)	quantiles 0-1, Moments 1-5

Appendix B: Image processing issues

The median filter may perform not satisfactorily, for instance when the background luminosity is changing rapidly (see Fig. B1).

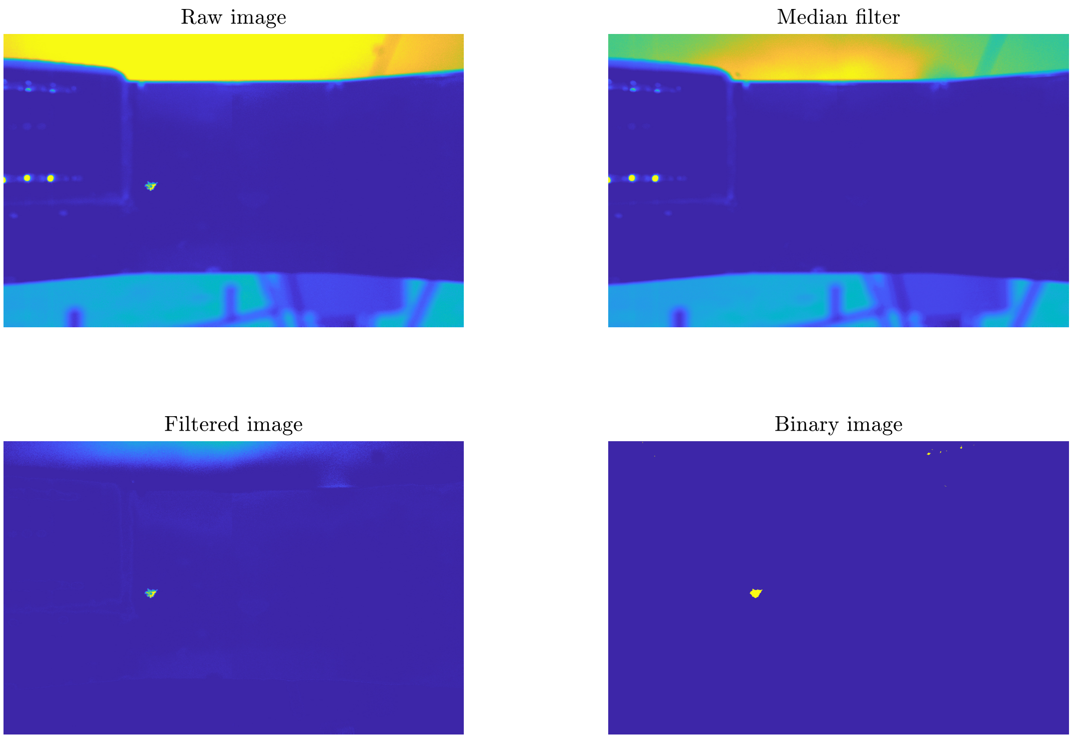

Figure B1. Raw image, median filter, filtered image and final binary image for an example where the median filter does not perform well due to changes in sky luminosity. Some artifacts appear on the top right of the binary image

Similarly, large ~~precipitaiton~~ precipitation particles may split or appear as such in the MASC images (see Fig. B2), leading to potential biases in the number of detected particles.

Code availability. TEXT

Data availability. TEXT

Code and data availability. The MASC images and the matlab codes used in the present work are available upon request to the authors.

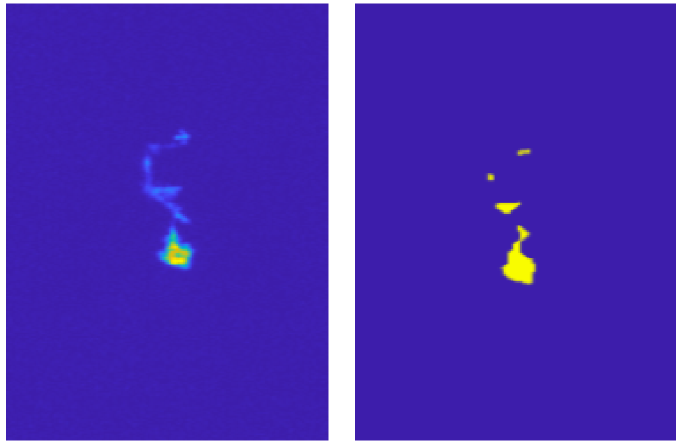

Figure B2. A precipitation particle split into fragments that could be confused with blowing snow particles. The Cumulative distance transform descriptor is much less affected by such image processing issues than the number of particles.

Sample availability. TEXT

Author contributions. TEXT

Competing interests. The authors have no competing interests

Disclaimer. TEXT

Acknowledgements. The authors are thankful to Yves-Alain Roulet and Jacques Grandjean from MeteoSwiss, as well as to Claudio Dùran from IGE Grenoble and to the technical staff at the Dumont d'Urville station for their help to collect the set of MASC images used in this study. CP was supported by the Swiss National Science Foundation (grant 200020_175700).

References

Bellot, H., Trouvilliez, A., Naaim-Bouvet, F., Genthon, C., and Gallée, H.: Present weather-sensor tests for measuring drifting snow, Adv. Geophys., 52, 176–184, 2011.

Bintanja, R.: Snowdrift sublimation in a katabatic wind region of the Antarctic ice sheet, J. Appl. Meteorol., 40, 1952–1966, https://doi.org/10.1175/1520-0450(2001)040<1952:SSIAKW>2.0.CO;2, 2001.

Box, J. E., Bromwich, D. H., Veenhuis, B. A., Bai, L.-S., Stroeve, J. C., Rogers, J. C., Steffen, K., Haran, T., and Wang, S.-H.: Greenland ice sheet surface mass balance variability (1988–2004) from calibrated polar MM5 output, J. Climate, 19, 2783–2800, 2006.

Byrt, T., Bishop, J., and Carlin, J. B.: Bias, prevalence and kappa, J. Clin. Epidemiol., 46, 423–429, 1993.

Comola, F., Kok, J. F., Gaume, J., Paterna, E., and Lehning, M.: Fragmentation of wind-blown snow crystals, Geophys. Res. Lett., 44, 4195–4203, 2017.

Crivelli, P., Paterna, E., Horender, S., and Lehning, M.: Quantifying particle numbers and mass flux in drifting snow, Bound.-Lay. Meterol., 161, 519–542, 2016.

Das, I., Bell, R. E., Scambos, T. A., Wolovick, M., Creyts, T. T., Studinger, M., Frearson, N., Nicolas, J. P., Lenaerts, J. T. M., and van den Broeke, M. R.: Influence of persistent wind scour on the surface mass balance of Antarctica, Nat. Geosci., 6, 367–371, https://doi.org/10.1038/NGEO1766, 2013.

De Maesschalck, R., Jouan-Rimbaud, D., and Massart, D. L.: The Mahalanobis distance, Chemometr. Intell. Lab., 50, 1–18, 2000.

Déry, S. J. and Yau, M.: Large-scale mass balance effects of blowing snow and surface sublimation, J. Geophys. Res., 107, ACL–8, 2002.

Ehbrecht, M., Schall, P., Ammer, C., and Seidel, D.: Quantifying stand structural complexity and its relationship with forest management, tree species diversity and microclimate, Agr. and Forest Meteor., 242, 1–9, 2017.

Gallée, H., Guyomarc'h, G., and Brun, E.: Impact of snow drift on the Antarctic ice sheet surface mass balance: possible sensitivity to snow-surface properties, Bound.-Lay. Meterol., 99, 1–19, 2001.

Garrett, T. J., Fallgatter, C., Shkurko, K., and Howlett, D.: Fall speed measurement and high-resolution multi-angle photography of hydrometeors in free fall, Atmos. Meas. Tech., 5, 2625–2633, https://doi.org/10.5194/amt-5-2625-2012, 2012.

Garrett, T. J., Yuter, S. E., Fallgatter, C., Shkurko, K., Rhodes, S. R., and Endries, J. L.: Orientations and aspect ratios of falling snow, Geophys. Res. Lett., 42, 4617–4622, 2015.

Genthon, C., Berne, A., Grazioli, J., Alarcon, C. D., Praz, C., and Boudevillain, B.: Precipitation at Dumont d'Urville, Adélie Land, East Antarctica: the APRES3 field campaigns dataset, Earth Syst. Sci. Data, 10, 1605–1612, https://doi.org/10.5194/essd-10-1605-2018, 2018.

Goodison, B. E., Louie, P. Y., and Yang, D.: WMO solid precipitation measurement intercomparison, World Meteorological Organization Geneva, Switzerland, 1998.

Gordon, M. and Taylor, P. A.: Measurements of blowing snow, Part I: Particle shape, size distribution, velocity, and number flux at Churchill, Manitoba, Canada, Cold Reg. Sci. Technol., 55, 63–74, 2009.

Gossart, A., Souverijns, N., Gorodetskaya, I. V., Lhermitte, S., Lenaerts, J. T., Schween, J. H., Mangold, A., Laffineur, Q., and van Lipzig, N. P.: Blowing snow detection from ground-based ceilometers: application to East Antarctica, The Cryosphere, 11, 2755, https://doi.org/10.5194/tc-11-2755-2017, 2017.

Grazioli, J., Genthon, C., Boudevillain, B., Duran-Alarcon, C., Del Guasta, M., Madeleine, J.-B., and Berne, A.: Measurements of precipitation in Dumont d'Urville, Adélie Land, East Antarctica, The Cryosphere, 11, 1797–1811, https://doi.org/10.5194/tc-11-1797-2017, https://www.the-cryosphere.net/11/1797/2017/, 2017.

Guyomarc'h, G., Bellot, H., Vionnet, V., Naaim-Bouvet, F., Déliot, Y., Fontaine, F., Puglièse, P., Nishimura, K., Durand, Y., and Naaim, M.: A meteorological and blowing snow data set (2000–2016) from a high-elevation alpine site (Col du Lac Blanc, France, 2720 m asl), Earth Syst. Sci. Data, 11, 57–69, 2019.

Kennedy, P., Thurai, M., Praz, C., Bringi, V., Berne, A., and Notaroš, B. M.: Variations in Snow Crystal Riming and Z DR: A Case Analysis, J. Appl. Meteor. Clim., 57, 695–707, 2018.

Kimura, F., Takashina, K., Tsuruoka, S., and Miyake, Y.: Modified quadratic discriminant functions and the application to Chinese character recognition, IEEE T. Pattern Anal., pp. 149–153, 1987.

Lehning, M. and Fierz, C.: Assessment of snow transport in avalanche terrain, Cold Reg. Sci. Technol., 51, 240–252, 2008.

Lenaerts, J. T. M. and van den Broeke, M. R.: Modeling drifting snow in Antarctica with a regional climate model: 2. Results, J. Geophys. Res., 117, https://doi.org/10.1029/2010JD015419, 2012.

Leonard, K. C., Tremblay, L.-B., Thom, J. E., and MacAyeal, D. R.: Drifting snow threshold measurements near McMurdo station, Antarctica: A sensor comparison study, Cold Reg. Sci. Technol., 70, 71–80, 2012.

Lesins, G., Bourdages, L., Duck, T., Drummond, J., Eloranta, E., and Walden, V.: Large surface radiative forcing from topographic blowing snow residuals measured in the High Arctic at Eureka, Atmos. Chem. Phys., 2009.

McGarigal, K. and Marks, B. J.: Spatial pattern analysis program for quantifying landscape structure, Tech. Rep. Gen. Tech. Rep. PNW-GTR-351, US Department of Agriculture, Forest Service, Pacific Northwest Research Station, 1995.

McLachlan, G. J. and Basford, K. E.: Mixture models: Inference and applications to clustering, vol. 84, Wiley Online Library, 1988.

Moerland, P.: Mixture models for unsupervised and supervised learning, 2000.

Mott, R. and Lehning, M.: Meteorological Modeling of Very High-Resolution Wind Fields and Snow Deposition for Mountains, JHM, 11, 934–949, https://doi.org/10.1175/2010JHM1216.1, 2010.

Murphy, K. P.: Machine Learning: A Probabilistic Perspective, MIT Press, 2012.

Naaim-Bouvet, F., Bellot, H., Nishimura, K., Genthon, C., Palerme, C., Guyomarc'h, G., and Vionnet, V.: Detection of snowfall occurrence during blowing snow events using photoelectric sensors, Cold Reg. Sci. Technol., 106, 11–21, 2014.

Nishimura, K. and Nemoto, M.: Blowing snow at Mizuho station, Antarctica, Philos. T. Roy. Soc. A, 363, 1647–1662, 2005.

Nishimura, K., Yokoyama, C., Ito, Y., Nemoto, M., Naaim-Bouvet, F., Bellot, H., and Fujita, K.: Snow particle speeds in drifting snow, J. Geophys. Res., 119, 9901–9913, 2014.

Palm, S. P., Yang, Y., Spinhirne, J. D., and Marshak, A.: Satellite remote sensing of blowing snow properties over Antarctica, J. Geophys. Res., 116, –, https://doi.org/10.1029/2011JD015828, 2011.

Pomeroy, J. and Li, L.: Prairie and arctic areal snow cover mass balance using a blowing snow model, J. Geophys. Res., 105, 26 619–26 634, 2000.

Praz, C., Roulet, Y.-A., and Berne, A.: Solid hydrometeor classification and riming degree estimation from pictures collected with a Multi-Angle Snowflake Camera, Atmos. Meas. Tech., 10, 1335–1357, https://doi.org/10.5194/amt-10-1335-2017, 2017.

Rasmussen, R., Baker, B., Kochendorfer, J., Meyers, T., Landolt, S., Fischer, A. P., Black, J., Thériault, J. M., Kucera, P., Gochis, D., Smith, C., Nitu, R., Hall, M., Ikeda, K., and Gutmann, E.: How well are we measuring snow: The NOAA/FAA/NCAR winter precipitation test bed, Bull. Amer. Meteor. Soc., 93, 811–829, https://doi.org/10.1175/BAMS-D-11-00052.1, 2012.

Scaff, L., Yang, D., Li, Y., and Mekis, E.: Inconsistency in precipitation measurements across the Alaska–Yukon border, The Cryosphere, 9, 2417–2428, 2015.

Scarchilli, C., Frezzotti, M., Grigioni, P., De Silvestri, L., Agnoletto, L., and Dolci, S.: Extraordinary blowing snow transport events in East Antarctica, Clim. Dynam., 34, 1195–1206, https://doi.org/10.1007/s00382-009-0601-0, 2010.

Schweizer, J., Bruce Jamieson, J., and Schneebeli, M.: Snow avalanche formation, Rev. Geophys., 41, 2003.

Shepherd, A., Ivins, E. R., Geruo, A., Barletta, V. R., Bentley, M. J., Bettadpur, S., Briggs, K. H., Bromwich, D. H., Forsberg, R., Galin, N., et al.: A reconciled estimate of ice-sheet mass balance, Science, 338, 1183–1189, 2012.

Winstral, A., Elder, K., and Davis, R. E.: Spatial snow modeling of wind-redistributed snow using terrain-based parameters, J. Hydrometeorol., 3, 524–538, 2002.

Yang, Y., Palm, S. P., Marshak, A., Wu, D. L., Yu, H., and Fu, Q.: First satellite- detected perturbations of outgoing longwave radiation associated with blowing snow events over Antarctica, Geophys. Res. Lett., 41, 730–735, https://doi.org/10.1002/2013GL058932, 2014.